Macromolecules

Article

pubs.acs.org/Macromolecules

# Cyclic Graft Copolymer Unimolecular Micelles: Effects of Cyclization on Particle Morphology and Thermoresponsive Behavior

Rebecca J. Williams,[†] Anaïs Pitto-Barry,[†] Nigel Kirby,[‡] Andrew P. Dove,*[,†] and Rachel K. O'Reilly*[,†]

[†]Department of Chemistry, University of Warwick, Gibbet Hill Road, Coventry CV4 7AL, U.K.

[‡]Australian Synchrotron, 800 Blackburn Road, Clayton, Victoria 3168, Australia

Supporting Information

**ABSTRACT:** The synthesis of cyclic amphiphilic graft copolymers with a hydrophobic polycarbonate backbone and hydrophilic poly(*N*-acryloylmorpholine) (PNAM) side arms via a combination of ring-opening polymerization (ROP), cyclization via copper-catalyzed azide−alkyne cycloaddition (CuAAC), and reversible addition−fragmentation chain transfer (RAFT) polymerization is reported. The ability of these cyclic graft copolymers to form unimolecular micelles in water is explored using a combination of light scattering, small-angle X-ray scattering (SAXS), and cryogenic transmission electron microscopy (cryoTEM) analyses, where particle size was found to increase with increasing PNAM arm length. Further analysis revealed differences in the solution conformations, loading capabilities, and morphologies of the cyclic graft copolymers in comparison to equivalent linear graft copolymer unimolecular micelle analogues. Furthermore, the cyclic and linear graft copolymers were found to exhibit significantly different cloud point temperatures. This study highlights how subtle changes in polymer architecture (linear graft copolymer versus cyclic graft copolymer) can dramatically influence a polymer's nanostructure and its properties.

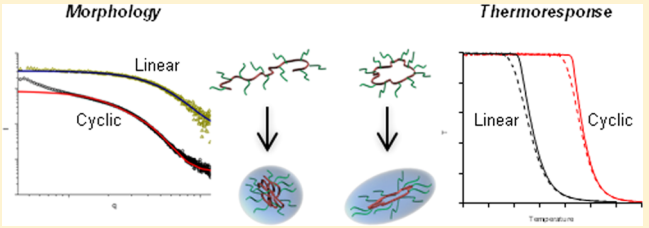


## INTRODUCTION

The function and properties of polymers are inherently linked to their structure; therefore, through variation of polymer composition and architecture a wide array of applications can be targeted.[1−3] Among the polymer architectures now available in the polymer chemist's toolbox are star,[4−6] branched,[7−10] and dendritic[11−13] structures as well as single chain polymer nanoparticles (SCNPs),[14−17] all of which have found application as unimolecular micelles for potential use as drug delivery vehicles.[10,13,18−20] These unimolecular particles possess advantages over conventional polymeric micelles prepared via the self-assembly of amphiphilic block copolymers,[21] where as a consequence of their unimolecular nature such particles do not display a critical micelle concentration, cannot disassemble, and demonstrate enhanced robustness toward variations in temperature, pH, and ionic strength. Furthermore, unimolecular micelles display a narrow particle size distribution, where the size and shape of the particles can be precisely controlled during polymer synthesis which allows for facile targeting of specific particle properties.

Polymers that possess a graft structure can also be utilized as unimolecular micelles, where the properties of these graft copolymers can be tailored via the systematic variation of arm length, backbone length, and grafting density, leading to an extremely versatile range of nanostructures.[5,22−25] Graft copolymers have been found to exhibit distinct self-assembly behavior in comparison to the conventional self-assembly of linear block copolymers; however, whereas the self-assembly of linear polymers is an extensive field of research,[21] the self-assembly of graft copolymers is relatively unexplored. Graft copolymers composed of a hydrophobic backbone and hydrophilic side arms are reported to form either unimolecular or multimolecular micelles upon dissolution in a selective solvent.[26−30] In a graft copolymer unimolecular micelle, the hydrophobic backbone collapses and is shielded from unfavorable solvent interactions by the hydrophilic side arms, resulting in a core−shell structure. Alternatively, graft copolymers self-assemble into loose micellar aggregates, where the aggregation number is typically low as a consequence of the increased number of hydrophilic blocks per hydrophobic block in comparison to assemblies composed of linear block copolymers. Whether graft copolymers self-assemble into unimolecular or multimolecular micelles is dependent on grafting density and the length and composition of the side arms and backbone, as these factors determine the interfacial tension between the hydrophobic backbone and solvated side arms and the repulsive interactions between side arms.

Another class of polymers that have received increased attention as a consequence of their architecture are those that possess a cyclic topology,[31−33] where cyclic polymers have been shown to exhibit some unique physical properties in comparison to their linear counterparts.[34−36] For example, cyclic polymers possess smaller hydrodynamic volumes and radii of gyration than analogous linear polymers as a result of

**Received:** December 15, 2015
**Revised:** February 17, 2016
**Published:** March 17, 2016

  

DOI: 10.1021/acs.macromol.5b02710
*Macromolecules* 2016, 49, 2802−2813

**Scheme 1. Synthesis of RAFT CTA-Functional Cyclic Polycarbonate Copolymers**

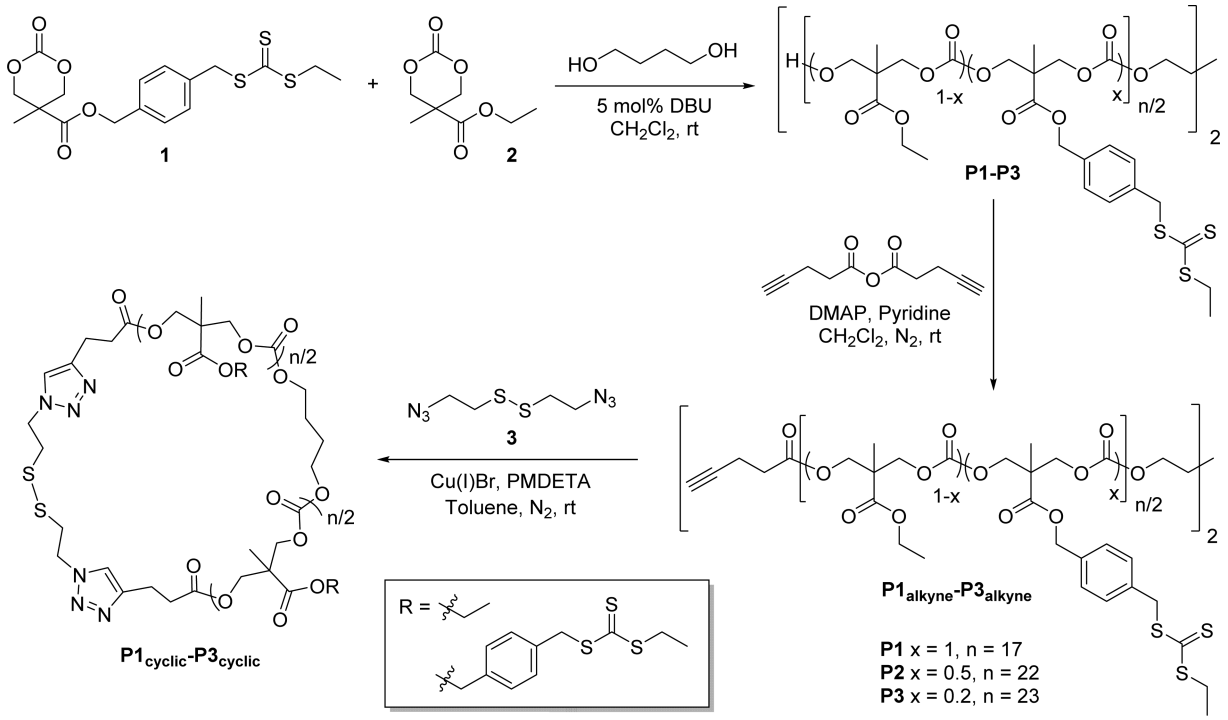


the more confined conformation of cyclic polymers. More recently, cyclic polymers have been shown to demonstrate some advantages over linear polymers when considered as potential drug or gene delivery vehicles. Grayson and co-workers reported that cyclic poly(ethylene imine) (PEI) displayed significantly higher transfection efficiencies in comparison to linear PEI,[37] while Yamamoto and Tezuka found that micelles assembled from cyclic diblock copolymers displayed greater robustness toward increasing temperature and ionic strength when compared to micelles composed of analogous linear triblock copolymers.[38,39] Furthermore, cyclic graft copolymers (graft copolymers that possess a cyclic backbone and linear side arms) have shown promise as carriers for tumor-targeted drug delivery.[40] Szoka and co-workers reported that poly(ethylene glycol) (PEG)-grafted cyclic copolymers display longer *in vivo* circulation times and higher tumor accumulation than equivalent PEG-grafted linear analogues.[41,42] Meanwhile, Pun and co-workers reported that folate-labeled poly(oligo ethylene glycol methacrylate) (POEGMA)-grafted cyclic copolymers display higher levels of specific targeted uptake into cancer cells compared to equivalent folate-labeled linear graft copolymers, suggesting that cyclic and linear graft copolymers follow different cell internalization mechanisms.[43]

Differences between the thermoresponsive behavior of cyclic and linear polymers that exhibit lower critical solution temperatures (LCSTs) have also been reported. However, there is some inconsistency as to the effect of cyclization on temperature response with some studies reporting that cyclic polymers display lower cloud point temperatures than equivalent linear polymers,[44−47] whereas other groups report that cloud point temperatures increase upon cyclization.[48−51] Moreover, the difference between cloud point temperatures of equivalent linear and cyclic polymers is only a few degrees (1−6 °C). In contrast, the difference in cloud point temperature of micellar assemblies composed of either linear or cyclic block copolymers is significantly larger. Yamamoto and Tezuka found that micelles assembled from cyclic poly(butyl acrylate)-*b*-poly(ethylene oxide) ($PBA_{12}$-*b*-$PEO_{59}$) displayed a cloud point temperature 40 °C higher than micelles prepared from linear $PBA_6$-*b*-$PEO_{59}$-*b*-$PBA_6$, despite both assemblies displaying comparable values of hydrodynamic diameter ($D_h$).[38] This large difference in cloud point temperature was attributed to the ability of the linear triblock copolymer to form intermicelle bridges resulting in particle agglomeration at lower temperatures, whereas the cyclic diblock copolymer micelles can only agglomerate through dehydration.

Following these reports, we wanted to explore the effect of cyclization on the solution properties and thermoresponsive behavior of unimolecular micelles prepared from amphiphilic graft copolymers. We anticipate that unimolecular micelles prepared from graft copolymers with a cyclic backbone will exhibit unique properties in comparison to those with a linear backbone. Our group has previously reported the synthesis of amphiphilic linear graft copolymers via a combination of ring-opening polymerization (ROP) and reversible addition−fragmentation chain transfer (RAFT) polymerization.[52] A novel RAFT chain transfer agent (CTA) functional cyclic carbonate monomer (**1**) was synthesized and polymerized via ROP before subsequent RAFT polymerization of *N*-isopropylacrylamide (NIPAM) to yield well-defined polycarbonate-*g*-poly(NIPAM) copolymers with a hydrophobic backbone and thermoresponsive hydrophilic side arms. In this article we expand this approach to prepare a range of thermoresponsive amphiphilic cyclic graft copolymers through a combination of ROP, cyclization via the copper-catalyzed azide−alkyne cycloaddition (CuAAC) "click" reaction, and RAFT polymerization. The aqueous solution properties of these amphiphilic cyclic graft copolymers are explored via laser light scattering, SAXS, and turbidimetry and compared to those of equivalent linear graft copolymers in order to ascertain the effect of polymer


DOI: 10.1021/acs.macromol.5b02710
*Macromolecules* 2016, 49, 2802−2813

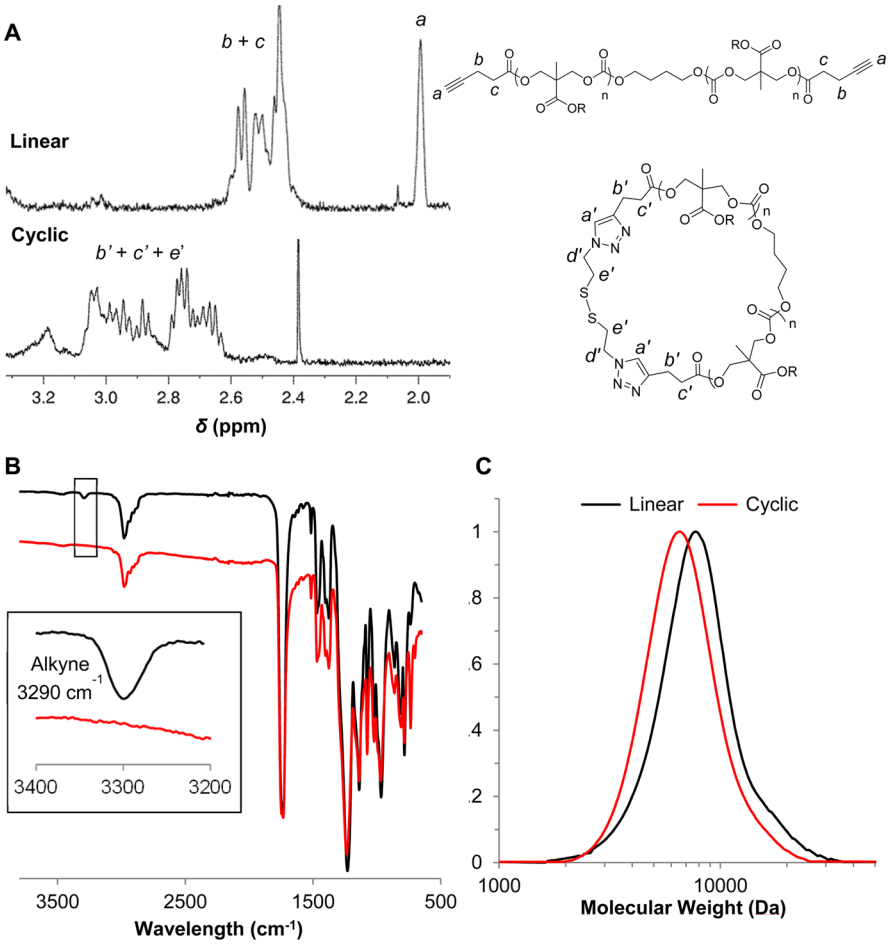


**Figure 1.** Characterization of alkyne-functional linear polycarbonate copolymer $\mathbf{P2}_{\mathbf{alkyne}}$ and cyclic polycarbonate copolymer $\mathbf{P2}_{\mathbf{cyclic}}$: (A) expansion of $^1$H NMR spectra (400 MHz, $CDCl_3$, $\delta$ = 3.3−1.9 ppm) of $\mathbf{P2}_{\mathbf{alkyne}}$ and $\mathbf{P2}_{\mathbf{cyclic}}$; (B) FT-IR spectra of $\mathbf{P2}_{\mathbf{alkyne}}$ (black) and $\mathbf{P2}_{\mathbf{cyclic}}$ (red), (inset) expansion of FT-IR spectra (3400−3200 $cm^{-1}$) highlighting loss of alkyne functionality; (C) size exclusion chromatograms for $\mathbf{P2}_{\mathbf{alkyne}}$ (black, $M_n$ = 7.4 kDa, $Đ_M$ = 1.17) and $\mathbf{P2}_{\mathbf{cyclic}}$ (red, $M_n$ = 6.2 kDa, $Đ_M$ = 1.16) in $CHCl_3$ with 0.5% $NEt_3$.

backbone architecture on thermoresponsive behavior and the use of amphiphilic graft copolymers as unimolecular micelles.

## RESULTS

**Synthesis of Cyclic Graft Copolymers.** Cyclic graft copolymers with a hydrophobic polycarbonate backbone and hydrophilic side arms were prepared through a combination of ring-closure and "grafting-from" approaches. Linear precursor polycarbonates were prepared via ROP and subsequently end-group modified before bimolecular ring-closure via CuAAC "click" chemistry (Scheme 1). Polymerization from RAFT CTA groups located on the cyclic polycarbonate backbone yielded cyclic graft copolymers.

Linear precursor polymers containing RAFT CTA functionalities were synthesized following our previously reported method for the organocatalyzed ring-opening copolymerization of the RAFT CTA-functional cyclic carbonate monomer **1** and ethyl-functional cyclic carbonate monomer, 5-methyl-5-ethoxycarbonyl-1,3-dioxan-2-one, **2** (Scheme 1).[52] Polymerizations were conducted in dichloromethane at room temperature using 5 mol% of 1,8-diazabicycloundec-7-ene (DBU) as the polymerization catalyst and 1,4-butanediol as the polymerization initiator to yield hydroxyl-terminated telechelic polycarbonates (initial monomer-to-initiator ratio = 25, [total monomer] = 0.25 M). The comonomer feed ratio (RAFT CTA-functional monomer **1**:ethyl-functional monomer **2**) was varied to target polycarbonates with 100% (1:0), 50% (1:1), and 20% (1:4) RAFT CTA functionality to obtain polymers **P1**, **P2**, and **P3**, respectively. Size exclusion chromatography (SEC) analysis of the resulting polycarbonate copolymers revealed monomodal molecular weight distributions with low dispersity values ($Đ_M \leq$ 1.2) (Figure S1), while $^1$H NMR spectroscopy revealed resonances that correspond to both the RAFT CTA and ethyl functionalities (Figure S2). Integration of these resonances allowed determination of the obtained incorporation of RAFT CTA functionality and revealed a strong agreement between the monomer feed ratio and the final copolymer composition. Furthermore, resonances that correspond to the $CH_2$ groups of the 1,4-butanediol initiating group at $\delta$ = 4.10 and 1.71 ppm were observed by $^1$H NMR spectroscopy. Matrix-assisted laser desorption ionization time-of-flight mass spectrometry (MALDI-ToF MS) of polymer **P1** with 100% RAFT CTA functionality revealed a single sodium-charged distribution with regular spacing equal to the molecular weight of the RAFT CTA-functional monomer repeat unit ($m/z$ = 400) and a 1,4-butanediol initiating group, confirming the excellent end-group fidelity of the polycarbonate and controlled nature of the polymerization (Table S1 and Figure S3).

The hydroxyl end-groups of the telechelic linear polycarbonates were transformed into alkyne functionalities via



DOI: 10.1021/acs.macromol.5b02710
Macromolecules 2016, 49, 2802−2813

esterification with an excess of 4-pentynoic anhydride, where quantitative functionalization was confirmed by $^1$H NMR spectroscopy, IR spectroscopy, and MALDI-ToF MS. Comparison of the $^1$H NMR spectra of the telechelic polycarbonates before and after functionalization revealed the appearance of a triplet resonance at $\delta$ = 1.97 ppm that corresponds to the terminal proton of the alkyne functionality and new resonances at $\delta$ = 2.58−2.37 ppm that correspond to the $CH_2$ groups adjacent to the alkyne moiety (Figure S4). The complete downfield shift of the resonance at $\delta$ = 3.70 ppm that corresponds to the $CH_2$ groups adjacent to the terminal hydroxyl functionalities was also observed. Examination of the IR spectra of the alkyne-functional telechelic polycarbonates showed the complete loss of the broad peak at 3540 cm$^{-1}$ that corresponds to the OH stretch of the hydroxyl end-groups and the appearance of a new signal at 3290 cm$^{-1}$ that corresponds to the CH stretch of the alkyne functionality (Figure S5). MALDI-ToF MS analysis of polymer $\mathbf{P1}_{\mathbf{alkyne}}$ further confirmed the quantitative functionalization of end-groups, revealing a single sodium charged distribution consistent with the successful esterification of both hydroxyl groups, observed as an increase in molecular weight of $m/z$ = 161 kDa (Figure S6). Furthermore, SEC analysis revealed that the molecular weight distribution of the polycarbonate copolymers remained narrow after end-group functionalization (Figure S7).

Cyclic RAFT CTA-functional polycarbonates were prepared through bimolecular ring closure via the copper-catalyzed cycloaddition of the alkyne-terminated telechelic polymers and a disulfide-containing diazide linker, **3**, which in turn was prepared according to adapted literature procedures.[53,54] To ensure cyclization was favored over step-growth polymerization, but also to reduce the quantity of solvent required, pseudo-high dilution[55] was used whereby a solution of linear precursor polymer and difunctional linker was slowly added to the catalyst solution via a syringe pump. A 100 mol excess of Cu(I) catalyst per mole of polymer was also used to ensure rapid ring-closure. Cyclization conditions were carefully optimized to enable effective bimolecular ring-closure; strictly stoichiometric quantities of diazide and difunctional alkyne polymer were used. Specifically, an equimolar solution of difunctional alkyne-terminated polycarbonate (1.0 mM) and diazide linker **3** in toluene were added via syringe pump to a stirred solution of Cu(I)Br (0.05 mM) and *N,N,N′,N″,N″*-pentamethyldiethylenetriamine (PMDETA) (0.05 mM) at room temperature at a rate of 0.3 mL h$^{-1}$. After complete addition of the polymer and diazide solution, the reaction was allowed to stir for a further 3 h. The copper catalyst was removed via washing with brine and then stirring the polymer solution overnight in the presence of CupriSorb beads. The polymer was isolated via precipitation into petroleum ether 40−60 °C. It was found that variation of these cyclization conditions, e.g., a faster rate of polymer and diazide addition or reduced dilution of the polymer, diazide, or catalyst solutions, resulted in significant polymer−polymer coupling as observed by SEC analysis (Figure S8). It was therefore concluded that high cyclization yields could only be achieved when ring closure was performed specifically under the optimized conditions.

A combination of characterization techniques were used to confirm the successful cyclization of the RAFT CTA-functional polycarbonates. $^1$H NMR spectroscopic analysis revealed the complete disappearance of the resonances attributed to the terminal proton of the alkyne functionality at $\delta$ = 1.97 ppm as well as a shift in the resonances that correspond to the adjacent $CH_2$ groups from $\delta$ = 2.58−2.37 ppm to $\delta$ = 3.06−2.58 ppm (Figure 1A and Figure S9). The appearance of resonances that correspond to the successful incorporation of the diazide disulfide linker were also observed, specifically the resonance at $\delta$ = 3.19 ppm that corresponds to the $CH_2$ groups adjacent to the disulfide moiety. The preservation of the quartet and triplet resonances at $\delta$ = 3.36 and 1.34 ppm, respectively, which correspond to the ethyl group of the RAFT CTA functionality, confirm that the RAFT CTA functionality was successfully retained during the CuAAC cyclization reaction. However, the $^1$H NMR spectra of the cyclized polycarbonates did not show the appearance of a resonance that corresponds to the proton of the triazole ring (Figure S9). It was hypothesized that this resonance was obscured by the aromatic signals at $\delta$ = 7.41−7.19 ppm from the RAFT CTA functionality. Indeed, when a cyclic polycarbonate was prepared from only ethyl-functional repeat units, $^1$H NMR spectroscopy revealed the appearance of a resonance at $\delta$ = 7.46 ppm that was attributed to the proton of the triazole ring (Figure S10). Analysis of the cyclized polymers by IR spectroscopy revealed the complete loss of signal at 3290 cm$^{-1}$ that corresponds to the CH stretch of the terminal alkyne groups (Figure 1B). Furthermore, signals at ca. 2100 cm$^{-1}$ which may correspond to azide functionality were not observed by IR spectroscopy, which indicates that chain blocking, where one polymer chain reacts with two diazide linker molecules preventing cyclization, had not occurred. Meanwhile, SEC analysis of the polycarbonates before and after cyclization revealed a reduction in apparent molecular weight as a consequence of the confined solution conformation of cyclic polymers in comparison to linear polymers (Table S3, Figure 1C, and Figure S11). Narrow molecular weight distributions and low dispersity values were also retained during ring closure, and the absence of any high molecular weight polymer impurities confirmed that polycondensation had not occurred. Examination of the MALDI-ToF mass spectrum of polymer $\mathbf{P1}_{\mathbf{cyclic}}$ provided further evidence of successful cyclization (Figure 2). An increase in molecular weight of $m/z$ = 204 Da was observed after cyclization, consistent with the addition of one equivalent of the diazide linker **3** per polymer chain.

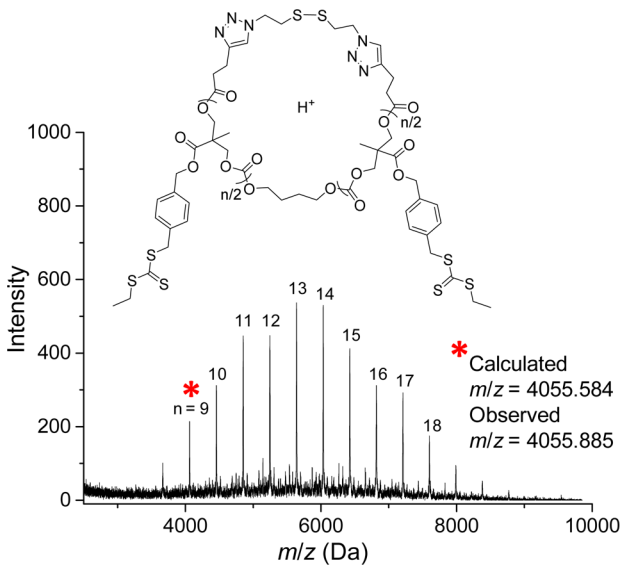


**Figure 2.** MALDI-ToF mass spectrum of cyclic polycarbonate $\mathbf{P1}_{\mathbf{cyclic}}$. Spectrum collected in linear mode.



DOI: 10.1021/acs.macromol.5b02710
*Macromolecules* 2016, 49, 2802−2813

**Scheme 2. Synthesis of *Cyclic*-Polycarbonate-*g*-PNAM Copolymers P4−P6 and *Linear*-Polycarbonate-*g*-PNAM Copolymers P7−P9**

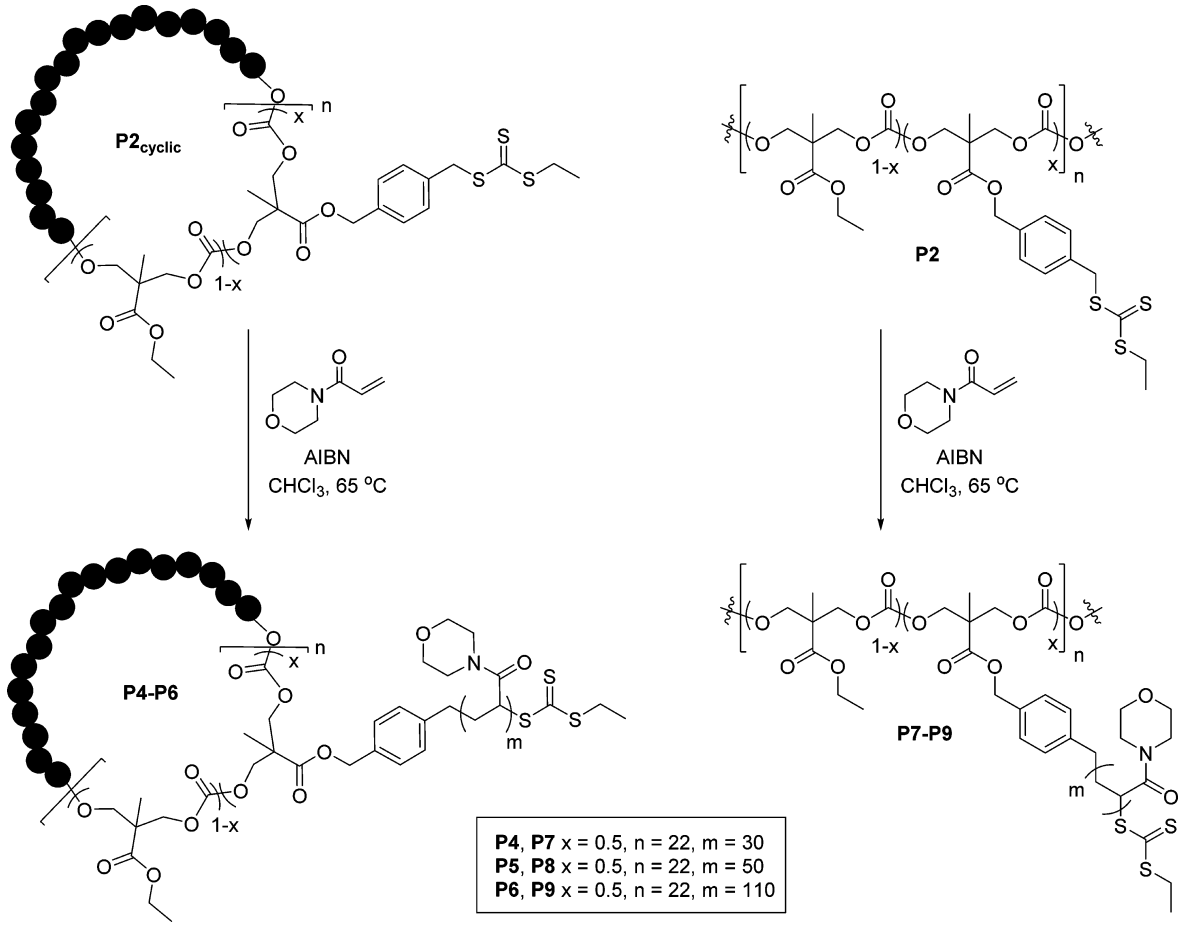


To prepare amphiphilic cyclic graft copolymers, hydrophilic poly(*N*-acryloylmorpholine) (PNAM) arms were grown from the RAFT CTA groups located on the cyclic polycarbonate backbone using similar conditions to those we previously reported for the preparation of linear graft copolymers (Scheme 2).[52] RAFT polymerizations were conducted at 65 °C in chloroform, with [starting polymer] = 3.0 mM and using 2,2′-azobis(isobutyronitrile) (AIBN) as the radical initiator. A ratio of [CTA]:[AIBN] = 1:0.1 was used, where the average number of CTA groups per polymer chain was determined by $^1$H NMR spectroscopy. The growth of PNAM arms from polymer **P2**$_{cyclic}$ (50% RAFT CTA functionality) was initially investigated using 100 equiv. of NAM per CTA unit. Following the polymerization SEC analysis revealed the presence of linear PNAM homopolymer impurities and the occurrence of graft−graft coupling at higher monomer conversions (>50%), as was also observed for the preparation of linear graft copolymers in our previous report (Figure S12).[52] Graft−graft coupling was eliminated by stopping polymerizations at low monomer conversion (<40%), and linear PNAM homopolymer contaminants were partially removed via dialysis to afford relatively well-defined amphiphilic cyclic graft copolymers ($Đ_M$ < 1.6). A range of *cyclic*-polycarbonate-*g*-PNAM copolymers with different PNAM arm lengths, from ca. DP 30 to DP 110, were prepared by varying the equivalents of NAM used during polymerization. The molecular weights of the resulting graft copolymers were observed to increase, from $M_n$ = 38.9 to 92.9 kDa, as PNAM arm length as evidenced by SEC analysis (Figure 3 and Table 1). Analysis of the *cyclic*-polycarbonate-*g*-PNAM copolymers by $^1$H NMR spectroscopy revealed resonances that correspond to both the PNAM arms and cyclic polycarbonate backbone—most notably the resonances at $\delta$ = 3.63 and 3.31 ppm attributed to the $CH_2$ groups of the morpholine ring and the resonances at $\delta$ = 4.27 and 1.24 ppm that correspond to the $CH_2$ and $CH_3$ groups of the polycarbonate backbone, respectively (Figure S13).

**Unimolecular Micelle Formation.** Following the successful synthesis of a range of amphiphilic cyclic graft copolymers their potential to form unimolecular micelles was investigated using multiple complementary characterization techniques: dynamic light scattering (DLS), static light scattering (SLS), small-angle X-ray scattering (SAXS), and cryogenic transmission electron microscopy (cryoTEM) (Table 2).[56] To allow comparison of their solution properties with linear graft copolymers, a range of *linear*-polycarbonate-*g*-PNAM copolymers (**P7−P9**) of equivalent compositions and molecular weights were also prepared by polymerization of NAM from linear polycarbonate **P2** (Table 1, Scheme 2, and Figure 3). Cyclic and linear graft copolymers **P4−P9** were all found to directly disperse in 18.2 MΩ·cm water, a selective solvent for the PNAM arms. We hypothesized that these amphiphilic graft copolymers would adopt a unimolecular core−shell micellar structure in aqueous solution to prevent unfavorable interactions between the hydrophobic polycarbonate backbone and the selective solvent for the NAM grafting block. $^1$H NMR spectroscopic analysis of **P4−P9** in $D_2O$ revealed that the


DOI: 10.1021/acs.macromol.5b02710
*Macromolecules* 2016, 49, 2802−2813

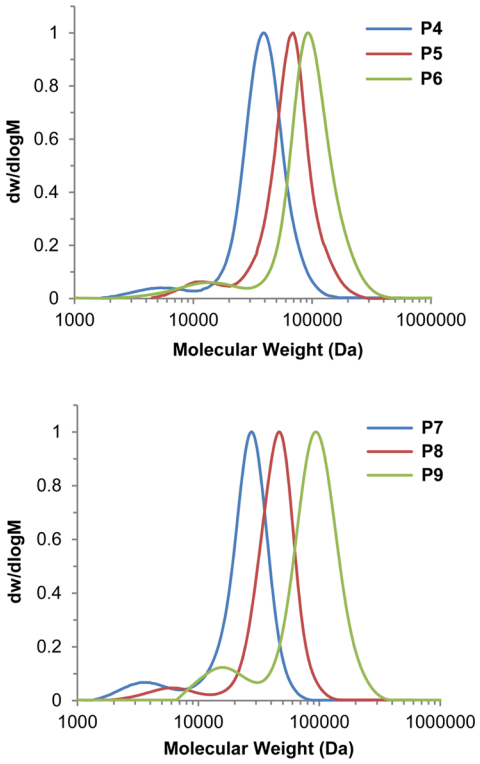


**Figure 3.** (top) Size exclusion chromatograms of *cyclic*-polycarbonate-*g*-PNAM copolymers **P4** ($M_n$ = 26.6 kDa, $Đ_M$ = 1.51), **P5** ($M_n$ = 45.3 kDa, $Đ_M$ = 1.47), and **P6** ($M_n$ = 60.5 kDa, $Đ_M$ = 1.66. (bottom) Size exclusion chromatograms of *linear*-polycarbonate-*g*-PNAM copolymers **P7** ($M_n$ = 15.8 kDa, $Đ_M$ = 1.62), **P8** ($M_n$ = 28.6 kDa, $Đ_M$ = 1.53), and **P9** ($M_n$ = 55.3 kDa, $Đ_M$ = 1.68), $CHCl_3$ with 0.5% $NEt_3$ as eluent and polystyrene standards.

**Table 1. Characterization of Cyclic and Linear Graft Copolymers P4−P9**

| polymer | structure | $M_n$(NMR)[a] (kDa) | $M_n$(SEC)[b] (kDa) | $M_p$(SEC)[b] (kDa) | $Đ_M$[b] |
|---|---|---|---|---|---|
| **P4** | *cyclic*-poly($\mathbf{2}_{11}$-*co*-$\mathbf{1}_{11}$-*g*-$NAM_{32}$) | 58.1 | 26.6 | 38.9 | 1.51 |
| **P5** | *cyclic*-poly($\mathbf{2}_{11}$-*co*-$\mathbf{1}_{11}$-*g*-$NAM_{50}$) | 86.8 | 45.3 | 69.2 | 1.47 |
| **P6** | *cyclic*-poly($\mathbf{2}_{11}$-*co*-$\mathbf{1}_{11}$-*g*-$NAM_{112}$) | 186 | 60.5 | 92.9 | 1.66 |
| **P7** | *linear*-poly($\mathbf{2}_{11}$-*co*-$\mathbf{1}_{11}$-*g*-$NAM_{28}$) | 51.3 | 15.8 | 27.7 | 1.62 |
| **P8** | *linear*-poly($\mathbf{2}_{11}$-*co*-$\mathbf{1}_{11}$-*g*-$NAM_{47}$) | 81.6 | 28.6 | 46.9 | 1.53 |
| **P9** | *linear*-poly($\mathbf{2}_{11}$-*co*-$\mathbf{1}_{11}$-*g*-$NAM_{112}$) | 185 | 55.3 | 93.0 | 1.68 |

[a]Determined by $^1$H NMR spectroscopy. [b]Determined by SEC analysis in $CHCl_3$ with 0.5% $NEt_3$ using polystyrene standards.

resonances that correspond to the $CH_2$ and $CH_3$ groups of the polycarbonate backbone at $\delta$ = 4.27 and 1.24 ppm were strongly attenuated, suggesting that the polycarbonate backbones of both the cyclic and linear graft copolymers are confined in a hydrophobic core (Figure S14). In contrast, for $^1$H NMR spectra recorded in $CDCl_3$ a good solvent for both the polycarbonate backbone and PNAM sides arms these resonances are clearly visible.

To determine whether confinement of the hydrophobic polycarbonate backbone is caused by adoption of a unimolecular core−shell structure or aggregation of the graft copolymers, DLS analysis of **P4−P9** was performed in both 18.2 MΩ·cm water, a selective solvent for the PNAM side arms, and 1,4-dioxane, a good solvent for both the side arms and polycarbonate backbone, at 4 mg $mL^{-1}$. Similar values of hydrodynamic diameter ($D_h$) were obtained in both solvents for linear and cyclic graft copolymers ($D_h$ = 7−12 nm), which indicated that the graft copolymers remained unimolecularly dispersed in water and did not assemble to form larger structures (Table 2). Moreover, the dispersities of the particles for both linear and cyclic graft copolymers in water were found to be <0.3, which indicates that the particles were relatively well-defined; however, a second population that corresponds to a slow mode of relaxation was observed in the intensity profile (Figures S15−S20). Further analysis of cyclic and linear graft copolymers **P6** and **P9** with the longest PNAM arm length of DP 110 by SLS also revealed two modes of relaxation. These two modes were separated using REPES analysis[57] where the slow modes of relaxation were found to be negligible through determination of the relative scattered intensities of the fast and slow modes. Molecular weight ($M_w$) and aggregation number ($N_{agg}$) were also determined via SLS analysis. Solutions of **P6** and **P9** were analyzed at a concentration of 4 mg $mL^{-1}$ at angles ranging from 30° to 150° in 18.2 MΩ cm water (Figures S21 and S22). The obtained values of $M_w$ for **P6** and **P9** were found to be 89.6 and 76.9 kDa, respectively, and the corresponding aggregation numbers ($N_{agg}$) were <1, providing further evidence of the unimolecular conformations of the cyclic and linear graft copolymers in water.

SAXS analysis of the cyclic and linear graft copolymers **P4−P9** in 18.2 MΩ cm water and 1,4-dioxane at 0.5 mg $mL^{-1}$ was also performed, and the radii of gyration ($R_g$) for the graft copolymers was determined using the Guinier−Porod model[58,59] available in the NCNR Analysis Macros in Igor Pro[60] (Figure S23). In agreement with DLS and SLS analysis, the linear and cyclic graft copolymers were not observed to aggregate into higher order structures in water but remained unimolecularly dispersed (Table 2). $R_g$ values from SAXS analysis were also determined using the AutoRg function available in Primus[61] to further confirm the values found using the Guinier−Porod fit in Igor (Table S4). When aggregation in the SAXS sample was not negligible (high turn of intensity at low $q$ values), the $R_g$ value was obtained by a manual fit and not an automatic fit to minimize the amount of aggregation in the modeling.

For both the cyclic and linear graft copolymers DLS analysis revealed that $D_h$ increased with increasing PNAM arm length, where polymers **P4** and **P7** with PNAM arm length of DP 30 displayed the smallest particle sizes (*cyclic*-**P4** $D_h$ = 7.6 nm, *linear*-**P7** $D_h$ = 6.7 nm) and polymers **P6** and **P9** with PNAM arm length of DP 110 displayed the largest particle sizes (*cyclic*-**P6** $D_h$ = 12 nm, *linear*-**P9** $D_h$ = 13 nm), demonstrating how particle size can be precisely tuned through variation of arm length (Table 2). Furthermore, values of $R_g$ determined by SAXS analysis were found to increase for both cyclic and linear graft copolymers as PNAM arm length was increased (Table 2 and Table S4).

The cyclic and linear graft copolymers with PNAM arm lengths of DP 110, **P6** and **P9**, respectively, were further analyzed by cryoTEM at a concentration of 2 mg $mL^{-1}$, which revealed the presence of particles and provided further evidence for the formation of micellar structures (Figure S24). The size of the particles corresponded to particle dimensions determined by light scattering and SAXS analysis suggesting


DOI: 10.1021/acs.macromol.5b02710
*Macromolecules* 2016, 49, 2802−2813

Table 2. DLS and SAXS Analysis of Cyclic and Linear Graft Copolymers P4−P9

| polymer | PNAM arm length | $D_h(H_2O)^a$ (nm) | $D_h$(dioxane)$^a$ (nm) | $R_g(H_2O)^b$ (nm) | $R_g$(dioxane)$^b$ (nm) | dimension parameter $(H_2O)^c$ | $R_g{}^b/R_h{}^a$ $(H_2O)$ |
|---|---|---|---|---|---|---|---|
| *cyclic*-**P4** | 30 | 7.6 ± 0.5 | 8.2 ± 0.1 | 3.3 ± 0.01 | 4.2 ± 0.01 | 0.18 | 0.87 |
| *linear*-**P7** | 30 | 6.7 ± 0.4 | 7.3 ± 0.5 | 2.7 ± 0.01 | 3.5 ± 0.01 | 0.20 | 0.81 |
| *cyclic*-**P5** | 50 | 10 ± 1 | 12 ± 1 | 4.3 ± 0.01 | 4.5 ± 0.01 | 0.65 | 0.86 |
| *linear*-**P8** | 50 | 7.7 ± 0.6 | 8.9 ± 0.4 | 3.5 ± 0.02 | 4.5 ± 0.05 | 0.16 | 0.91 |
| *cyclic*-**P6** | 110 | 12 ± 0.4 | 13 ± 0.5 | 5.7 ± 0.01 | 4.7 ± 0.17 | 0.29 | 0.95 |
| *linear*-**P9** | 110 | 13 ± 0.4 | 14 ± 0.3 | 5.8 ± 0.01 | *d* | 0.27 | 0.89 |

[a]Determined by DLS analysis, concentration 4 mg mL$^{-1}$. [b]Determined by SAXS analysis using the Guinier−Porod model in Igor software, concentration 0.5 mg mL$^{-1}$. [c]Determined by the Guinier−Porod model; 0 means spherical micelles, 1 is for rodlike micelles, and 2 is for platelike micelles. The model is more accurate for hard micelles but can still give information for softer or looser assemblies. [d]Poor sample collection did not provide raw data of good quality.

that both the PNAM arms and polycarbonate core were visible, where cyclic graft copolymer **P6** displayed an average particle diameter ($D_{av}$) of 17.7 ± 6 nm and $D_{av}$ = 12.9 ± 3 nm for linear graft copolymer **P9**. Particles of cyclic graft copolymer **P6** appeared to be clustered together, which may explain the aggregation observed at low $q$ values for this polymer during SAXS analysis.

**Effect of Backbone Architecture on Unimolecular Micelle Conformation.** Investigation of the solution properties of graft copolymers **P4−P9** revealed distinct differences between those with a cyclic polycarbonate backbone and those with a linear polycarbonate backbone. Whereas the nongrafted cyclic polycarbonates (**P1**$_{cyclic}$−**P3**$_{cyclic}$) displayed lower apparent molecular weights as determined by SEC analysis than the equivalent nongrafted linear polycarbonates (**P1**−**P3**) (a phenomena which is well-known and occurs as a consequence of the reduced conformational freedom of cyclic polymers) (Figure S10 and Table S3), the cyclic and linear graft copolymers with DP 30 and DP 50 PNAM arm lengths were found to exhibit the opposite trend. Cyclic graft copolymers **P4** and **P5** displayed a greater apparent molecular weight than the equivalent linear graft copolymers (**P7** and **P8**) (Figure 4 and Table 1), suggesting that these cyclic graft copolymers possess a larger hydrodynamic volume than the equivalent linear graft copolymers. Meanwhile, the cyclic and linear graft copolymers with the longest PNAM arm length (**P6** and **P9**) were found to display very similar values of apparent molecular weight. This trend in hydrodynamic volume between cyclic and linear graft copolymers was also observed by DLS and SAXS analysis, where values of $D_h$ and $R_g$ were observed to be larger for the cyclic graft copolymers **P4** and **P5** in comparison to the linear graft copolymers **P7** and **P8** in both water and 1,4-dioxane, whereas cyclic and linear graft copolymers with PNAM arm length of DP 110 (**P6** and **P9**) displayed similar values of $D_h$ and $R_g$ (Table 2).

The ability to load the hydrophobic polycarbonate core of the graft copolymer unimolecular micelles was investigated to determine whether the observed differences in hydrodynamic volume between the cyclic and linear graft copolymers affected their ability to uptake the hydrophobic dye Nile Red. Aqueous solutions of cyclic and linear graft copolymers **P4−P9** (1 mg mL$^{-1}$) were added to an excess of Nile Red and stirred for 16 h before filtration to remove unsequestered dye. The polymer solutions were analyzed by UV−vis spectroscopy which revealed the appearance of a signal at $\lambda$ = 550 nm that corresponds to encapsulated Nile Red (Figure 4). The cyclic graft copolymers were found to uptake more Nile Red than the equivalent linear graft copolymers, suggesting either that the volume of hydrophobic polycarbonate core of the cyclic graft copolymers was larger than the linear graft copolymers or that the hydrophobic core of the cyclic graft copolymers was more accessible than the core of the linear graft copolymer particles.

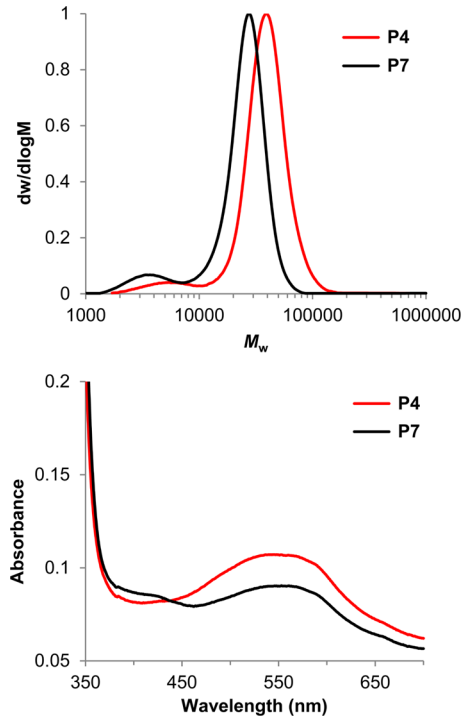


**Figure 4.** (left) Size exclusion chromatograms of *cyclic*-poly(**2**$_{11}$-*co*-**1**$_{11}$-*g*-NAM$_{32}$) (**P4**) and *linear*-poly(**2**$_{11}$-*co*-**1**$_{11}$-*g*-NAM$_{28}$) (**P7**), $CHCl_3$ with 0.5% $NEt_3$ as eleunt. (right) UV−vis spectra of **P4** and **P7** in 18.2 MΩ cm (1 mg mL$^{-1}$) after incubation with an excess of Nile Red.

Further differences between the solution conformations of unimolecular micelles prepared from *cyclic*- and *linear*-polycarbonate-*g*-PNAM copolymers were revealed by SAXS analysis, where a range of complex structural models based on shape form factors of scattering objects were used to model the SAXS data. As a consequence of the graft structure of the polymers and their deviation into a unimolecular core−shell structure, Debye and polydisperse Gaussian coil models did not provide a good fit for the data for either cyclic or linear graft copolymers. For both cyclic and linear graft copolymers with the shortest PNAM arm length (DP 30, **P4** and **P7**) a spherical micelle model with some dispersity on the radius (PolyCore-Form model,[62] Figure 5) was found to fit well. Further evidence that graft copolymers **P4** and **P7** possessed a spherical morphology was obtained by determination of a dimension parameter, a measure of the anisotropy of the unimolecular


DOI: 10.1021/acs.macromol.5b02710
Macromolecules 2016, 49, 2802−2813

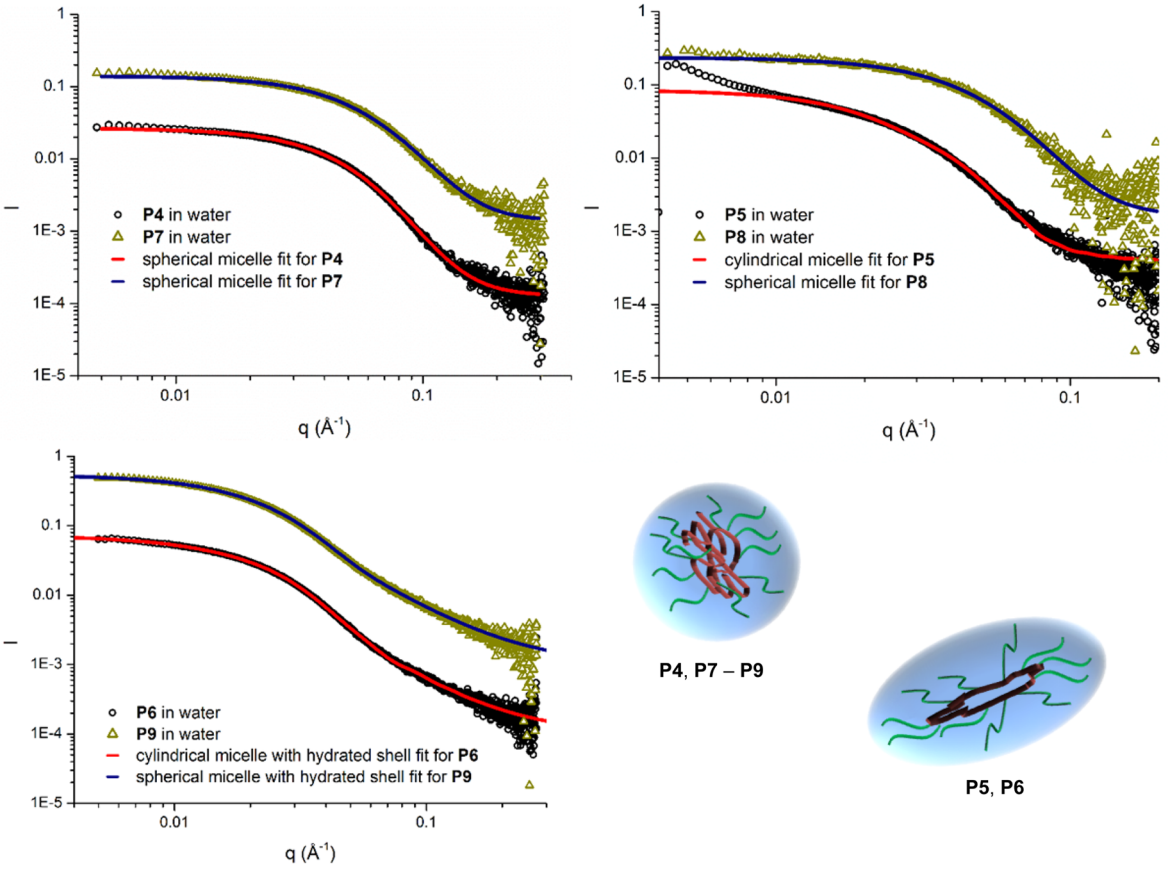


**Figure 5.** (top left) SAXS profiles and corresponding spherical micelle fits for polymers **P4** and **P7** in 18.2 MΩ cm water. Data for **P7** have been shifted vertically by a factor 10 for more clarity. (top right) SAXS profiles and corresponding cylindrical and spherical micelle fits for polymers **P5** and **P8** in 18.2 MΩ cm water. Data for **P8** have been shifted vertically by a factor 20 for more clarity. (bottom left) SAXS profiles and corresponding cylindrical and spherical micelle fits for polymers **P6** and **P9** in 18.2 MΩ cm water. Data for **P9** have been shifted vertically by a factor 10 for more clarity. (bottom right) Schematic representation of cyclic (**P4**–**P6**) and linear (**P7**–**P9**) graft copolymers adopting spherical and cylindrical conformations.

micelles, using the Guinier–Porod model (where a value of zero is indicative of a spherical structure, a value of 1 indicates a rodlike morphology, and a value of 2 indicates a platelike structure). Both cyclic and linear graft copolymers with a PNAM arm length of DP 30 displayed dimension parameters close to zero (*cyclic*-**P4** 0.18, *linear*-**P7** 0.20), indicating these unimolecular micelles possessed a spherical morphology.

When PNAM arm length was increased to DP 50, a deviation between the solution conformation of the cyclic and linear graft copolymer micelles was observed. Whereas linear graft copolymer **P8** was found to fit well to a spherical micelle model, the equivalent cyclic graft copolymer **P5** fitted well to a cylindrical model with dispersity on the radius (Cypr model,[58] Figure 5). This observation was further supported by determination of the dimension parameters for **P5** and **P8**; while the linear graft copolymer with PNAM arm length of DP 50 possessed a dimension parameter close to zero (*linear*-**P8** 0.16), the dimension parameter of the cyclic graft copolymer with DP 50 PNAM arm length (**P5**) was found to be 0.65, suggestive of a more elongated structure. Moreover, the slope of the SAXS data in the Porod region ($q$ values between 0.006 and 0.02 Å$^{-1}$) for **P5** was determined to be −0.94, which is very close to −1, the value expected for a rodlike morphology (Figure S25 and Table S5).

A difference in solution morphology between cyclic and linear graft copolymers with PNAM arm length of DP 110 (**P6** and **P9**) was also observed by SAXS analysis; however, fitting this data proved difficult. While uniform and core–shell models of spherical and cylindrical micelles provided either no fit or a very poor fit for cyclic graft copolymer **P6**, the best fit was observed for a linear summation of a uniform cylindrical micelle model and a model for polymeric chains in a good solvent (Polydisperse Gaussian Coils).[63,64] We have previously demonstrated that a similar summation model (PolyCoreForm model and Debye model for monodisperse polymer chains in a good solvent) provides a good fit for particles in the presence of a hydrated shell that could not be accounted for by fitting with a core–shell model.[65] Therefore, cyclic graft copolymer **P6** behaves as a cylindrical micelle with a hydrated PNAM shell, where the summation model provides a cylindrical length of 17.8 nm with a core radius of 5.0 nm and a shell thickness of 13.9 nm (Figure 5). Kratky plots were used to gain more information on the morphology of **P6** (Figure S26). The plot for spheres ($Iq^2$ vs $q$) exhibits a horizontal asymptote at high $q$ values, indicative of a spherical morphology in solution. However, as there is almost no shape observed at low $q$ values for this Kratky plot, the possibility that the particles present a different morphology cannot be discarded. Meanwhile, the Kratky plot for rods ($Iq^2$ vs $q$) also displays a horizontal asymptote in combination with a well-defined symmetrical bell-shaped curve at low $q$ values, which strongly indicates the presence of a rodlike morphology in solution. The bell-like


DOI: 10.1021/acs.macromol.5b02710
*Macromolecules* 2016, 49, 2802–2813

shape has a maximum intensity at $q$ = 0.17 Å$^{-1}$, which corresponds to a repeat unit length of 37 nm. This correlates with the longer dimension found for the form factor fit (radius of core and thickness of shell of 18.9 nm, therefore a total diameter of 37.8 nm). The low-intensity bell shape obtained for the spherical Kratky plot has a maximum intensity at $q$ = 0.028 Å$^{-1}$, a repeat unit length of 22 nm, which is in good agreement with the length provided by the form factor fit (17.8 nm). The slope of the SAXS raw data in the Porod region for **P6** was found to be −0.81, which further indicates that a rodlike morphology is more likely to be observed (Figure S25 and Table S5).

In contrast, the linear graft copolymer with DP 110 PNAM arms (**P9**) exhibits the behavior of a spherical micelle with a hydrated shell. Again, the hydrated PNAM shell could not be accounted for using the core−shell models available in Igor; neither a spherical nor cylindrical model could fit the raw data at high $q$ values. Thus, a linear summation of a uniform spherical model and a model for polymeric chains in a good solvent (Polydisperse Gaussian Coils) was used to provide further information on the sample (Figure 5). The summation model afforded a core radius of 5.5 nm and a shell thickness of 11.4 nm. A linear summation with a cylindrical model was also attempted but did not provide a good fit. Despite the morphological differences observed between the cyclic and linear graft copolymers with DP 110 PNAM arm length (**P6** and **P9**) by SAXS analysis, the dimension parameters for **P6** and **P9** were found to be very similar (*cyclic*-**P6** 0.29, *linear*-**P9** 0.27) and suggestive of a slightly anisotropic morphology.

The ratio $R_g/R_h$ is related to the spatial density distribution of a polymer or particle in solution and gives an indication of nanostructure morphology, where $R_g/R_h$ = 0.775 indicates a solid sphere or fully collapsed globule, $R_g/R_h$ = 1 a hollow sphere, $R_g/R_h$ = 1.5 a random coil in a good solvent, and $R_g/R_h$ > 2 a rodlike chain or elongated structure. Values of $R_g/R_h$ in 18.2 MΩ cm water were determined for the cyclic and linear graft copolymers, where $R_g$ and $R_h$ were determined by SAXS using the Guinier−Porod model and DLS analysis, respectively. For all cyclic and linear graft copolymers (**P4**−**P9**), $R_g/R_h$ ranged from 0.81 to 0.95, indicating these unimolecular micelles possessed a partially collapsed spherical structure (Table 2). This result was slightly unexpected for cyclic graft copolymers **P5** and **P6**, where SAXS analysis suggested the particles possessed a slightly elongated structure; however, when $R_g/R_h$ was determined using $R_g$ from the Primus analysis, values of 1.37 and 1.36 were obtained, consistent with elongated structures (Table S4).

Comparison of the values of $R_g$ determined by the Guinier−Porod and AutoRg models can provide further insight into the anisotropy of the graft copolymer particles. Whereas the Guinier−Porod model provides a value of $R_g$ that corresponds to the cross section of the particle, the Primus model provides a value of $R_g$ that corresponds to an intermediate value between the cross section and the length of the particle; for spherical particles these values should be very similar, whereas for anisotropic particles these two values of $R_g$ will vary. For linear graft copolymers **P7**−**P9** (PNAM arm lengths of DP 30, 50, and 110, respectively) and cyclic graft copolymer **P4** (PNAM arm length of DP 30) the values of $R_g$ determined using the two models in Igor and Primus were found to be in close agreement (Table 2 and Table S4), providing further evidence that these unimolecular particles possessed a spherical morphology. Meanwhile, for cyclic graft copolymers **P5** and **P6** (PNAM arm lengths of DP 50 and 110, respectively) values of $R_g$ determined using the two different models showed significant variation (Table 2 and Table S4), providing further evidence that these polymers adopted an elongated conformation in solution in accordance with the aforementioned SAXS analyses.

Overall, detailed SAXS analysis of the cyclic and linear graft copolymers in combination with DLS analysis revealed distinct differences between their solution conformations. Both the cyclic and linear graft copolymers adopt a unimolecular micellar structure in aqueous solution, and for short PNAM arm lengths these particles are observed to be spherical. However, as PNAM arm length is increased from DP 30 to DP 110, the cyclic graft copolymer particles adopt a more elongated morphology, whereas the linear graft copolymers remain spherical, across the polymer compositions studied.

**Effect of Backbone Architecture on Thermoresponsive Properties.** To determine whether the conformational differences observed between the cyclic and linear graft copolymers affect their macroscopic properties, the thermoresponsive behavior of graft copolymers **P4**−**P9** was investigated. In aqueous solution PNAM homopolymer does not exhibit an observable cloud point; however, the phase transition temperatures of polymers that display LCSTs can be lowered through the introduction of hydrophobicity to the polymer chain, as such low molecular weight telechelic PNAM with hydrophobic end-groups has been reported to display cloud point temperatures ranging from 45 to 80 °C, dependent on end-group identity.[66,67] Polymers with a grafted architecture are also known to display lower phase transition temperatures as a consequence of the close proximity of their side arms.[68,69] Therefore, the grafted architecture of **P4**−**P9** and the presence of the hydrophobic polycarbonate backbone may lower the LCST of the PNAM side arms, resulting in an observable cloud point.

The cloud point temperatures of cyclic and linear graft copolymers **P4**−**P9** in 18.2 MΩ cm water were determined spectrophotometrically by measuring the turbidity of the solutions at 1 mg mL$^{-1}$, with a 1 °C min$^{-1}$ heating and cooling rate. Large differences (ca. 20 °C) were observed between the cloud point temperatures of the cyclic and linear graft copolymers and as expected the cloud point temperatures of both the cyclic and linear graft copolymers increased as PNAM arm length and consequently the hydrophilic character of the graft copolymers increased. For graft copolymers with a PNAM arm length of DP 30, the linear graft copolymer **P7** displayed a cloud point temperature of 47 °C, whereas the cloud point temperature for the equivalent cyclic graft copolymer **P4** was significantly higher at 67 °C (Figure 6). A small amount of hysteresis was observed during the cooling cycles for both cyclic and linear graft copolymers. For graft copolymers with PNAM arm lengths of DP 50 the cloud point temperature of the linear graft copolymer **P8** was found to be 74 °C; however, no cloud point was observed below 90 °C for the equivalent cyclic graft copolymer **P5** (Figure S27). Meanwhile, no cloud points were observed below 90 °C for both cyclic and linear graft copolymers with PNAM arm lengths of DP 110 (**P6** and **P9**). The dramatic difference in cloud point temperatures between cyclic and linear graft copolymers provides further evidence of their different solution conformations and the effect this can have on their macroscopic properties. Interestingly, this difference did not correlate to a change in the morphology of the particles as graft copolymers **P4** and **P7** with PNAM arm length DP 30, both observed to


DOI: 10.1021/acs.macromol.5b02710
*Macromolecules* 2016, 49, 2802−2813

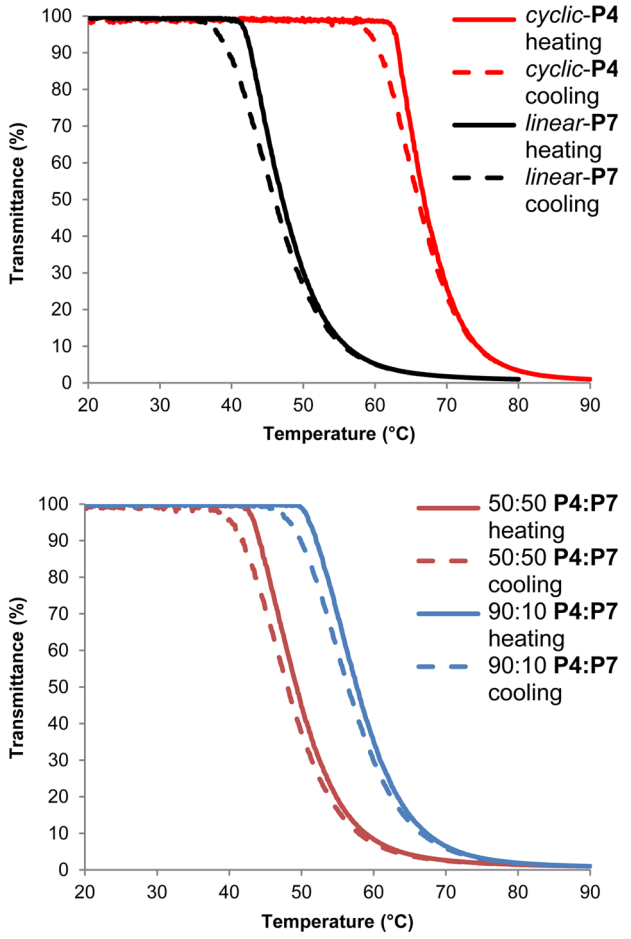


**Figure 6.** Percentage transmittance (%) against temperature (°C) for (top) *cyclic*-poly($\mathbf{2}_{11}$-*co*-$\mathbf{1}_{11}$-*g*-$NAM_{32}$) (**P4**) and *linear*-poly($\mathbf{2}_{11}$-*co*-$\mathbf{1}_{11}$-*g*-$NAM_{28}$) (**P7**) and (bottom) 50:50 and 90:10 mixtures of **P4**:**P7** at 1 mg $mL^{-1}$ in 18.2 MΩ cm water; heating/cooling rate = 1 °C $min^{-1}$.

possess a similar spherical morphology by SAXS analysis, exhibited very different cloud point temperatures. We therefore propose that this large variation occurs as a consequence of the larger hydrodynamic volumes of the cyclic graft copolymers in comparison to the linear graft copolymers, resulting in a greater number of interactions between the cyclic graft copolymers and water; thus, dehydration and agglomeration occur at higher temperatures. Furthermore, the differences observed in cloud point temperature between the cyclic and linear graft copolymers are significantly larger than cloud point temperature differences observed between nongrafted cyclic and linear polymers reported previously in the literature.[44−51] This difference may result from the relatively large molecular weights of the polymers in this work compared to previous studies, therefore emphasizing differences in cloud point temperature, and in contrast to previous work this unprecedented difference in cloud point temperature allows us to observe the definitive effect of cyclization on temperature response for this system.

Solutions of cyclic graft copolymer **P4** and linear graft copolymer **P7** were mixed together in different ratios (50:50 and 90:10 **P4**:**P7**) in an attempt to tune cloud point temperature.[70] The resulting solutions were found to exhibit a single cloud point transition indicating that the cyclic and linear graft copolymers displayed cooperative thermoresponsive behavior. Interestingly, the resulting cloud point temperatures of the mixtures were not proportional to the ratio of each polymer. For the 50:50 mixture the cloud point temperature was 49 °C, very close to that of pure linear graft copolymer **P7** (Figure 6). Meanwhile, the cloud point temperature for the 90:10 mixture was 58 °C approximately halfway between the cloud point temperatures of pure cyclic and linear graft copolymers, demonstrating how small quantities of linear graft copolymer contaminants can dramatically affect the cloud point temperature of the cyclic graft copolymer. Again, as a consequence of the large and significant difference between the cloud point temperatures of the cyclic and linear graft copolymers the effect of mixing can be clearly observed. This is in contrast to conventional nongrafted systems where the cloud points of cyclic and linear polymers are very similar and the effects of mixing would be less evident.

## CONCLUSIONS

A series of amphiphilic cyclic graft copolymers with a hydrophobic polycarbonate backbone and hydrophilic PNAM side arms were prepared via a combination of ROP, CuAAC cyclization, and RAFT polymerization. These cyclic graft copolymers and their linear graft copolymer analogues were demonstrated to form unimolecular micelles when dispersed in water, where particles size could be precisely tuned by variation of PNAM arm length. Detailed structural characterization of the unimolecular assemblies revealed distinct differences between the size, morphology, and properties of the cyclic and linear graft copolymers. For short PNAM arm lengths, cyclic graft copolymers exhibited larger particle dimensions and greater loading capacities than the equivalent linear graft copolymers. As PNAM arm length increased, differences between the morphologies of cyclic and linear graft copolymer particles were also observed; the cyclic graft copolymer particles switched from a spherical to a cylindrical conformation as PNAM arm length increased whereas the linear graft copolymer particles remained spherical. Investigation of the thermoresponsive properties of the graft copolymers also revealed a significant variation in cloud point temperatures between cyclic and linear polymers. This research highlights important differences between cyclic and linear graft copolymers which affects their behavior as unimolecular micelles and should be considered in the future development of these materials as drug carriers.

## ASSOCIATED CONTENT

### Supporting Information

The Supporting Information is available free of charge on the ACS Publications website at DOI: 10.1021/acs.macromol.5b02710.

Experimental procedures, additional polymer characterization data, DLS, SLS, and SAXS data (PDF)

## AUTHOR INFORMATION

### Corresponding Authors

*E-mail a.p.dove@warwick.ac.uk; Fax +44 024 7652 4112; Tel +44 024 7652 4107 (A.P.D.).

*E-mail: r.k.o-reilly@warwick.ac.uk; Fax +44 024 7652 4112; Tel +44 024 7652 3236 (R.K.O.).

### Notes

The authors declare no competing financial interest.



DOI: 10.1021/acs.macromol.5b02710
*Macromolecules* 2016, 49, 2802−2813

## ■ ACKNOWLEDGMENTS

Mr. Ian Hands-Portman is thanked for assistance with cryo-TEM. The Royal Society is thanked for the award of an Industry Fellowship to A.P.D. EPSRC and ERC are also acknowledged for funding to support R.K.O.

## ■ REFERENCES

(1) Gregory, A.; Stenzel, M. H. Complex polymer architectures via RAFT polymerization: From fundamental process to extending the scope using click chemistry and nature's building blocks. *Prog. Polym. Sci.* **2012**, *37*, 38−105.
(2) Hadjichristidis, N.; Iatrou, H.; Pitsikalis, M.; Mays, J. Macromolecular architectures by living and controlled/living polymerizations. *Prog. Polym. Sci.* **2006**, *31*, 1068−1132.
(3) Hirao, A.; Goseki, R.; Ishizone, T. Advances in Living Anionic Polymerization: From Functional Monomers, Polymerization Systems, to Macromolecular Architectures. *Macromolecules* **2014**, *47*, 1883−1905.
(4) Blencowe, A.; Tan, J. F.; Goh, T. K.; Qiao, G. G. Core cross-linked star polymers via controlled radical polymerisation. *Polymer* **2009**, *50*, 5−32.
(5) Deng, Y.; Zhang, S.; Lu, G.; Huang, X. Constructing well-defined star graft copolymers. *Polym. Chem.* **2013**, *4*, 1289−1299.
(6) Khanna, K.; Varshney, S.; Kakkar, A. Miktoarm star polymers: advances in synthesis, self-assembly, and applications. *Polym. Chem.* **2010**, *1*, 1171−1185.
(7) England, R. M.; Rimmer, S. Hyper/highly-branched polymers by radical polymerisations. *Polym. Chem.* **2010**, *1*, 1533−1544.
(8) Gao, H.; Matyjaszewski, K. Synthesis of functional polymers with controlled architecture by CRP of monomers in the presence of cross-linkers: From stars to gels. *Prog. Polym. Sci.* **2009**, *34*, 317−350.
(9) Voit, B. I.; Lederer, A. Hyperbranched and Highly Branched Polymer Architectures—Synthetic Strategies and Major Characterization Aspects. *Chem. Rev.* **2009**, *109*, 5924−5973.
(10) Zhu, X.; Zhou, Y.; Yan, D. Influence of branching architecture on polymer properties. *J. Polym. Sci., Part B: Polym. Phys.* **2011**, *49*, 1277−1286.
(11) Carlmark, A.; Hawker, C.; Hult, A.; Malkoch, M. New methodologies in the construction of dendritic materials. *Chem. Soc. Rev.* **2009**, *38*, 352−362.
(12) Inoue, K. Functional dendrimers, hyperbranched and star polymers. *Prog. Polym. Sci.* **2000**, *25*, 453−571.
(13) Soliman, G. M.; Sharma, A.; Maysinger, D.; Kakkar, A. Dendrimers and miktoarm polymers based multivalent nanocarriers for efficient and targeted drug delivery. *Chem. Commun.* **2011**, *47*, 9572−9587.
(14) Gonzalez-Burgos, M.; Latorre-Sanchez, A.; Pomposo, J. A. Advances in single chain technology. *Chem. Soc. Rev.* **2015**, *44*, 6122−6142.
(15) Altintas, O.; Barner-Kowollik, C. Single-Chain Folding of Synthetic Polymers: A Critical Update. *Macromol. Rapid Commun.* **2016**, *37*, 29−46.
(16) Lyon, C. K.; Prasher, A.; Hanlon, A. M.; Tuten, B. T.; Tooley, C. A.; Frank, P. G.; Berda, E. B. A brief user's guide to single-chain nanoparticles. *Polym. Chem.* **2015**, *6*, 181−197.
(17) Hansell, C. F.; Lu, A.; Patterson, J. P.; O'Reilly, R. K. Exploiting the tetrazine-norbornene reaction for single polymer chain collapse. *Nanoscale* **2014**, *6*, 4102−4107.
(18) Fox, M. E.; Szoka, F. C.; Fréchet, J. M. J. Soluble Polymer Carriers for the Treatment of Cancer: The Importance of Molecular Architecture. *Acc. Chem. Res.* **2009**, *42*, 1141−1151.
(19) Gao, H. Development of Star Polymers as Unimolecular Containers for Nanomaterials. *Macromol. Rapid Commun.* **2012**, *33*, 722−734.
(20) Gillies, E. R.; Fréchet, J. M. J. Dendrimers and dendritic polymers in drug delivery. *Drug Discovery Today* **2005**, *10*, 35−43.
(21) Mai, Y.; Eisenberg, A. Self-assembly of block copolymers. *Chem. Soc. Rev.* **2012**, *41*, 5969−5985.
(22) Feng, C.; Li, Y.; Yang, D.; Hu, J.; Zhang, X.; Huang, X. Well-defined graft copolymers: from controlled synthesis to multipurpose applications. *Chem. Soc. Rev.* **2011**, *40*, 1282−1295.
(23) Rzayev, J. Molecular Bottlebrushes: New Opportunities in Nanomaterials Fabrication. *ACS Macro Lett.* **2012**, *1*, 1146−1149.
(24) Sheiko, S. S.; Sumerlin, B. S.; Matyjaszewski, K. Cylindrical molecular brushes: Synthesis, characterization, and properties. *Prog. Polym. Sci.* **2008**, *33*, 759−785.
(25) Uhrig, D.; Mays, J. Synthesis of well-defined multigraft copolymers. *Polym. Chem.* **2011**, *2*, 69−76.
(26) Hadjichristidis, N.; Roovers, J. Conformation of poly(isoprene-gstyrene) in dilute solution. *J. Polym. Sci., Polym. Phys. Ed.* **1978**, *16*, 851−858.
(27) Pispas, S.; Hadjichristidis, N.; Mays, J. W. Micellization of Model Graft Copolymers of the H and $\pi$ Type in Dilute Solution. *Macromolecules* **1996**, *29*, 7378−7385.
(28) Pitsikalis, M.; Woodward, J.; Mays, J. W.; Hadjichristidis, N. Micellization of Model Graft Copolymers in Dilute Solution. *Macromolecules* **1997**, *30*, 5384−5389.
(29) Price, C.; Woods, D. Light-scattering study of micelle formation by polystyrene-g-polyisoprene graft copolymers. *Polymer* **1974**, *15*, 389−392.
(30) Tuzar, Z.; Kratochvil, P.; Procházka, K.; Contractor, K.; Hadjichristidis, N. Solution behavior of a graft copolymer in selective solvents for its backbone or grafts. *Makromol. Chem.* **1989**, *190*, 2967−2973.
(31) Jia, Z.; Monteiro, M. J. Cyclic polymers: Methods and strategies. *J. Polym. Sci., Part A: Polym. Chem.* **2012**, *50*, 2085−2097.
(32) Kricheldorf, H. R. Cyclic polymers: Synthetic strategies and physical properties. *J. Polym. Sci., Part A: Polym. Chem.* **2010**, *48*, 251−284.
(33) Laurent, B. A.; Grayson, S. M. Synthetic approaches for the preparation of cyclic polymers. *Chem. Soc. Rev.* **2009**, *38*, 2202−2213.
(34) Williams, R. J.; Dove, A. P.; O'Reilly, R. K. Self-assembly of cyclic polymers. *Polym. Chem.* **2015**, *6*, 2998−3008.
(35) Yamamoto, T.; Tezuka, Y. Topological polymer chemistry: a cyclic approach toward novel polymer properties and functions. *Polym. Chem.* **2011**, *2*, 1930−1941.
(36) Yamamoto, T.; Tezuka, Y. Cyclic polymers revealing topology effects upon self-assemblies, dynamics and responses. *Soft Matter* **2015**, *11*, 7458−7468.
(37) Cortez, M. A.; Godbey, W. T.; Fang, Y.; Payne, M. E.; Cafferty, B. J.; Kosakowska, K. A.; Grayson, S. M. The Synthesis of Cyclic Poly(ethylene imine) and Exact Linear Analogues: An Evaluation of Gene Delivery Comparing Polymer Architectures. *J. Am. Chem. Soc.* **2015**, *137*, 6541−6549.
(38) Honda, S.; Yamamoto, T.; Tezuka, Y. Topology-Directed Control on Thermal Stability: Micelles Formed from Linear and Cyclized Amphiphilic Block Copolymers. *J. Am. Chem. Soc.* **2010**, *132*, 10251−10253.
(39) Honda, S.; Yamamoto, T.; Tezuka, Y. Tuneable enhancement of the salt and thermal stability of polymeric micelles by cyclized amphiphiles. *Nat. Commun.* **2013**, *4*, 1574.
(40) Wang, C. E.; Stayton, P. S.; Pun, S. H.; Convertine, A. J. Polymer nanostructures synthesized by controlled living polymerization for tumor-targeted drug delivery. *J. Control. Release* **2015**, *219*, 345−354.
(41) Chen, B.; Jerger, K.; Fréchet, J. M. J.; Szoka, F. C., Jr. The influence of polymer topology on pharmacokinetics: Differences between cyclic and linear PEGylated poly(acrylic acid) comb polymers. *J. Control. Release* **2009**, *140*, 203−209.
(42) Nasongkla, N.; Chen, B.; Macaraeg, N.; Fox, M. E.; Fréchet, J. M. J.; Szoka, F. C. Dependence of Pharmacokinetics and Biodistribution on Polymer Architecture: Effect of Cyclic versus Linear Polymers. *J. Am. Chem. Soc.* **2009**, *131*, 3842−3843.
(43) Wei, H.; Wang, C. E.; Tan, N.; Boydston, A. J.; Pun, S. H. ATRP Synthesis of Sunflower Polymers Using Cyclic Multimacroinitiators. *ACS Macro Lett.* **2015**, *4*, 938−941.



DOI: 10.1021/acs.macromol.5b02710
*Macromolecules* 2016, 49, 2802−2813

(44) Xu, J.; Ye, J.; Liu, S. Synthesis of Well-Defined Cyclic Poly(N-isopropylacrylamide) via Click Chemistry and Its Unique Thermal Phase Transition Behavior. *Macromolecules* **2007**, *40*, 9103−9110.
(45) Ye, J.; Xu, J.; Hu, J.; Wang, X.; Zhang, G.; Liu, S.; Wu, C. Comparative Study of Temperature-Induced Association of Cyclic and Linear Poly(N-isopropylacrylamide) Chains in Dilute Solutions by Laser Light Scattering and Stopped-Flow Temperature Jump. *Macromolecules* **2008**, *41*, 4416−4422.
(46) Lahasky, S. H.; Hu, X.; Zhang, D. Thermoresponsive Poly(α-peptoid)s: Tuning the Cloud Point Temperatures by Composition and Architecture. *ACS Macro Lett.* **2012**, *1*, 580−584.
(47) Liu, B.; Wang, H.; Zhang, L.; Yang, G.; Liu, X.; Kim, I. A facile approach for the synthesis of cyclic poly(N-isopropylacrylamide) based on an anthracene-thiol click reaction. *Polym. Chem.* **2013**, *4*, 2428−2431.
(48) Qiu, X.-P.; Tanaka, F.; Winnik, F. M. Temperature-Induced Phase Transition of Well-Defined Cyclic Poly(N-isopropylacrylamide)s in Aqueous Solution. *Macromolecules* **2007**, *40*, 7069−7071.
(49) Qiu, X.-P.; Winnik, F. M. Effect of Topology on the Properties of Poly(N-isopropylacrylamide) in Water and in Bulk. *Macromol. Symp.* **2009**, *278*, 10−13.
(50) Satokawa, Y.; Shikata, T.; Tanaka, F.; Qiu, X.-p.; Winnik, F. M. Hydration and Dynamic Behavior of a Cyclic Poly(N-isopropylacrylamide) in Aqueous Solution: Effects of the Polymer Chain Topology. *Macromolecules* **2009**, *42*, 1400−1403.
(51) Yuan, Y.-Y.; Du, J.-Z.; Wang, J. Two consecutive click reactions as a general route to functional cyclic polyesters. *Chem. Commun.* **2012**, *48*, 570−572.
(52) Williams, R. J.; O'Reilly, R. K.; Dove, A. P. Degradable graft copolymers by ring-opening and reverse addition-fragmentation chain transfer polymerization. *Polym. Chem.* **2012**, *3*, 2156−2164.
(53) Wang, Y.; Zhang, R.; Xu, N.; Du, F.-S.; Wang, Y.-L.; Tan, Y.-X.; Ji, S.-P.; Liang, D.-H.; Li, Z.-C. Reduction-Degradable Linear Cationic Polymers as Gene Carriers Prepared by Cu(I)-Catalyzed Azide−Alkyne Cycloaddition. *Biomacromolecules* **2011**, *12*, 66−74.
(54) Withey, A. B. J.; Chen, G.; Nguyen, T. L. U.; Stenzel, M. H. Macromolecular Cobalt Carbonyl Complexes Encapsulated in a Click-Cross-Linked Micelle Structure as a Nanoparticle To Deliver Cobalt Pharmaceuticals. *Biomacromolecules* **2009**, *10*, 3215−3226.
(55) Laurent, B. A.; Grayson, S. M. An Efficient Route to Well-Defined Macrocyclic Polymers via "Click" Cyclization. *J. Am. Chem. Soc.* **2006**, *128*, 4238−4239.
(56) Patterson, J. P.; Robin, M. P.; Chassenieux, C.; Colombani, O.; O'Reilly, R. K. The analysis of solution self-assembled polymeric nanomaterials. *Chem. Soc. Rev.* **2014**, *43*, 2412−2425.
(57) Jakeš, J. *Collect. Czech. Chem. Commun.* **1995**, *60*, 1781−1797.
(58) Guinier, A.; Fournet, G. *Small-Angle Scattering of X-Rays*; John Wiley and Sons: New York, 1955.
(59) Glatter, O.; Kratky, O. *Small-Angle X-ray Scattering*; Academic Press: London, 1982; pp 155−156.
(60) Kline, S. Reduction and analysis of SANS and USANS data using IGOR Pro. *J. Appl. Crystallogr.* **2006**, *39*, 895−900.
(61) Petoukhov, M. V.; Franke, D.; Shkumatov, A. V.; Tria, G.; Kikhney, A. G.; Gajda, M.; Gorba, C.; Mertens, H. D. T.; Konarev, P. V.; Svergun, D. I. New developments in the ATSAS program package for small-angle scattering data analysis. *J. Appl. Crystallogr.* **2012**, *45*, 342−350.
(62) Bartlett, P.; Ottewill, R. H. A neutron scattering study of the structure of a bimodal colloidal crystal. *J. Chem. Phys.* **1992**, *96*, 3306−3318.
(63) Higgins, J. S.; Benoît, H. C. In *Polymers and Neutron Scattering*; Oxford series on neutron scattering in condensed matter 8; Oxford Science Publications: 1996; pp 158−161.
(64) Glatter, O.; Kratky, O. In *Small-angle X-ray Scattering*; Academic Press: London, 1982; pp 403−407.
(65) Wright, D. B.; Patterson, J. P.; Pitto-Barry, A.; Lu, A.; Kirby, N.; Gianneschi, N. C.; Chassenieux, C.; Colombani, O.; O'Reilly, R. K. The Copolymer Blending Method: A New Approach for Targeted Assembly of Micellar Nanoparticles. *Macromolecules* **2015**, *48*, 6516−6522.
(66) Sawada, H.; Kawase, T.; Ikematsu, Y.; Ishii, Y.; Oue, M.; Hayakawa, Y. Synthesis and surfactant properties of novel fluoroalkylated amphiphilic oligomers. *Chem. Commun.* **1996**, 179−180.
(67) Sawada, H.; Takahashi, K.; Mugisawa, M.; Oya, T.; Ogino, S.-i. Thermoresponsive Characteristics of Fluoroalkyl End-Capped Co-oligomers in Aqueous Solutions and on the Poly(methyl methacrylate) Film Surface. *Langmuir* **2007**, *23*, 11947−11950.
(68) Theato, P.; Sumerlin, B. S.; O'Reilly, R. K.; Epps, T. H., III Stimuli responsive materials. *Chem. Soc. Rev.* **2013**, *42*, 7055−7056.
(69) Gibson, M. I.; O'Reilly, R. K. To aggregate, or not to aggregate? considerations in the design and application of polymeric thermally-responsive nanoparticles. *Chem. Soc. Rev.* **2013**, *42*, 7204−7213.
(70) Ieong, N. S.; Hasan, M.; Phillips, D. J.; Saaka, Y.; O'Reilly, R. K.; Gibson, M. I. Polymers with molecular weight dependent LCSTs are essential for cooperative behaviour. *Polym. Chem.* **2012**, *3*, 794−799.


DOI: 10.1021/acs.macromol.5b02710
*Macromolecules* 2016, 49, 2802−2813